Chemical Engineering Science 247 (2022) 117071

Contents lists available at ScienceDirect

Chemical Engineering Science

journal homepage: www.elsevier.com/locate/ces

Breakup behavior of a shear-thinning droplet on randomly rough surfaces: A numerical study

Hongtao Xia, Xiaofang Zhang, Jie Xiao *

Particle Engineering Laboratory, School of Chemical and Environmental Engineering, College of Chemistry, Chemical Engineering and Materials Science, Soochow University, Suzhou, Jiangsu Province 215123, China

HIGHLIGHTS

- Breakup threshold of non-Newtonian droplets impacting on randomly rough surfaces.
- Deposition state as a function of Weber number and surface roughness.
- Critical Weber number is more sensitive to root-mean-square roughness than to Wenzel roughness.
- Numerically identified critical velocity that can ensure a non-splashing state.

ARTICLE INFO

Article history:
Received 12 May 2021
Received in revised form 5 August 2021
Accepted 29 August 2021
Available online 01 September 2021

Keywords:
Droplet impact
Receding breakup
Fingering splash
Critical Weber number
Randomly rough surfaces
Phase field method

ABSTRACT

Surface roughness has been known to facilitate droplet breakup, but the effects of surface morphology on the breakup threshold have not yet been quantitatively clarified. In this paper, numerical simulations are carried out to investigate the fate of a shear-thinning droplet impacting on specially designed randomly rough surfaces. By resorting to a total of 1380 in-silico experiments, deposition state diagrams are constructed, which can offer three types of state as a function of the Weber number and the surface morphology quantified by the root-mean-square roughness (Rr) and the Wenzel roughness parameter (Wr). Results show that it is Rr rather than Wr that can effectively promote droplet splash. Furthermore, critical velocities that can ensure a non-splashing state are identified for different sized droplets impacting on surfaces with different morphologies. This quantitative information has great potential to facilitate operational optimization in a wide range of applications demanding non-splash droplets.

1. Introduction

The phenomenon of a droplet impacting on a rough surface has always been a highly researched topic in the field of fluid dynamics, being of great importance in a wide variety of agricultural and engineering practices, such as crop spraying (Bergeron et al., 2000; Wirth et al., 1991), spray coating (Li et al., 2007; Xiao et al., 2010), ink-jet printing (Dam and Clerc, 2004), and forensic research (Adam, 2013; Li et al., 2021; Smith et al., 2018).

In internal combusting engines, the evaporation, combustion and, emission of fuel oil is heavily influenced by droplet impact. For ink-jet printing, the droplets impacting the surface should not splash in order to obtain the optimal printing quality. In some cases, the droplets break up, forming satellite droplets depending on the nozzle geometry and ink properties, which greatly affects the printing quality (Dong et al., 2014). In the automobile industry, a complex spraying method is used to paint vehicles. This process faces a variety of technical challenges, as the quality of the final coating can be affected by the slight imperfection of the initial surface. The case of spray painting of vehicle panels, can be described as a process where a liquid film is formed by many tiny droplets impacting on a solid surface. It is extremely difficult to ensure a uniform coating if the paint-based droplets are broken upon impact, forming a number of secondary droplets, which can negatively affect the appearance and aesthetics of vehicle coatings. The challenging and important task of controlling the coating quality can be facilitated by using simulations. Xiao et al. (2018) have previously used the phase field method to simulate the deposition process of paint-based droplets on random rough surfaces, however, the splashing processes have yet to be explored.

Droplet impact dynamics are influenced by the liquid properties, impact parameters, and substrate properties and topology. The dynamics can be categorized as droplet deposition without breakup, corona splash, prompt splash, fingering splash, receding breakup and, partial or complete rebound (Allen, 1975; Chen

* Corresponding author.
E-mail address: jie.xiao@suda.edu.cn (J. Xiao).

https://doi.org/10.1016/j.ces.2021.117071
0009-2509/

Nomenclature

$\boldsymbol{F}$	volume force vector ($N \cdot m^{-3}$)
g	gravity vector ($m \cdot s^{-2}$)
G	chemical potential ($J \cdot m^{-3}$)
h_i	height of the data point (m)
$\bar{h}$	mean height of all n data points (m)
m	the consistency coefficient ($Pa \cdot s^n$)
n	power law index
M	mobility ($m^3 \cdot s \cdot kg^{-1}$)
p	pressure (Pa)
Re	Reynolds number
Rr	root-mean-square roughness (μm)
u	velocity ($m \cdot s^{-1}$)
u_0	velocity of impact ($m \cdot s^{-1}$)
We	Weber number
Wr	Wenzel roughness

Greek letters

α	volume fraction
ε	interface thickness (m)
θ_b	contact angle (°)
λ	mixing energy density (N)
ρ	density ($kg \cdot m^{-3}$)
σ	surface tension ($N \cdot m^{-1}$)
ϕ	dimensionless phase-field parameter
χ	mobility tuning parameter ($m \cdot s \cdot kg^{-1}$)

et al., 2018; Cossali et al., 1997; Cossali et al., 2008; Marengo et al., 2011; Mehdizadeh and Chandra, 2004; Moita and Moreira, 2007; Roisman et al., 2002). The fingering splash, and receding breakup are two common breakup results, which become main focuses of this paper. Thoroddsen et al. (2005) showed that droplet fingers can either split during the spreading process due to the presence of trapped air under the droplet, resulting in a fingering splash, or merge during the recoiling process. Pan et al. (2010) concluded in their study that a receding breakup occurs when a droplet finger, or lamella with little inertia is unable to merge with the central droplet during the recoiling process. The Weber number, which characterizes the ratio of impact inertia to surface tension, has been used to describe droplet splashing threshold in most of experimental and theoretical studies:

$$We = \frac{\rho D_0 u_0^2}{\sigma} \tag{1}$$

where ρ and σ are the liquid density and surface tension respectively; D_0, u_0 are the initial droplet diameter and impact velocity. Wachters and Westerling (1966) investigated the normal impact of a droplet (2.3 mm in diameter) on a hot gold wall and identified a critical Weber number of 80, above which the drop disintegrates upon impact. Based on findings by Wachters and Westerling (1966) and others, Wang and Watkins (1993) modelled diesel spray impingement on walls and proposed that a diesel droplet, after impacting a solid wall, would either rebound, or stick and shatter on the wall, depending on the impact energy, with We = 80 as the critical condition of shattering. Stow and Hadfield (1981) and Mundo et al. (1995) used another parameter, K, to determine the splashing/non-splashing outcomes,

$$K = We \cdot Re^{\frac{1}{2}} \tag{2}$$

$$Re = \frac{\rho D_0 u_0}{\mu} \tag{3}$$

where μ is the viscosity of the liquid. Splashing occurs when K is above a critical K_c, which was obtained through the fitting of experimental data, however, no general agreement exists on the correlation between K_c and surface roughness. Latka et al. (2012) and Lei et al. (2005) showed that a corona splash can only be observed for very smooth surfaces. They used a constant critical capillary number, Ca, as the splash threshold.

$$\mathrm{Ca} = \frac{We}{Re} \tag{4}$$

Wal et al. (2006) used liquid droplets of various viscosities for impact experiments onto a very smooth substrate. Therein, splashing upon impact on a dry surface can be reasonably described by, reflecting the competing roles of surface tension and viscosity. Riboux and Gordillo (2014) deduced a criterion to determine the critical velocity for which deposition or corona splash occurs on a smooth dry surface.

Most of the studies mentioned above focused on droplet splashing on a smooth surface, but in reality, most solid surfaces are randomly rough. The dynamic study of droplet impact on smooth or patterned surfaces rather than randomly rough surfaces must deviate from real life situations. The study of droplet impact on a randomly rough surface is much more challenging than that on a controlled surface, resulting in a limited number of studies on the droplet splashing process on randomly rough surfaces. Lei et al. (2005) and Li et al. (2010) showed that prompt splashing takes place on a rough surface, where secondary droplets are emitted from the breakup of the liquid rim just after the impact. Roisman et al. (2015) found that on rough surfaces the main parameters that induce splashing are the roughness of substrate and the impact Weber number. They have proposed an empirical correlation for the prompt splash on rough and porous substrates based on their experimental data. Kai and Feuillebois (1998) criterion for splash threshold was based on a critical Weber number, which depends on the surface roughness. Tan (2017) carried out 3D simulations of splashing of micrometer-sized water droplets on dry micro-structured surfaces. Their findings showed that both initial impact velocity and surface morphology play an important role in droplet splashing.

A tremendous volume of analytical, experimental and, numerical studies have investigated droplet splashing; however, the splashing model has not yet been tested for complex fluids. Non-Newtonian fluids are very common in industry and daily life, including asphalt, suspensions such as blood, and some food items such as ketchup, creams etc. The research on non-Newtonian fluids will benefit many industrial fields, having more practical significance, and a higher application value. Bertola and Haw (2015) developed a volume of fluid (VOF) model to simulate a fuel droplet impacting and splashing on a wetted surface. The simulation results showed that the pressure gradient inside liquid was the main factor influencing droplet behavior. Smith et al., 2018 investigated the influence of surface roughness and wettability on the splashing limit of droplets of blood, a non-Newtonian colloidal fluid; they found that surface roughness plays a far more major role in the threshold of the splashing/non-splashing behavior of blood compared to the wettability. Chen et al. (2018) demon-

strated that the induced non-Newtonian elongational viscosity causes strong energy dissipation, while the elasticity of polymer chains slows down droplet retraction and increases the contact time of rebounding. de Goede et al. (2018) investigated the effects of surface wetting properties and the surface tension of the liquid on the splashing velocity of the droplet, however, blood was modeled as a Newtonian fluid while it was subjected to high shear rates in that study.

The aforementioned studies show that research on the dynamic splashing process of non-Newtonian fluid droplets on randomly rough surfaces is limited. Even though the deposition dynamics of both Newtonian and non-Newtonian fluids on randomly rough surfaces have been investigated (Zhang et al., 2014; Xiao et al., 2018; Xia et al., 2019), they were limited to droplet deposition without breakup. In order to improve our understanding of droplet splashing, research on the splashing process of non-Newtonian fluid droplets on randomly rough surfaces is of urgent need. In this work, a numerical model based on the phase field method was developed to identify the splashing threshold of shear-thinning droplets on randomly rough surfaces. Systematic analyses were then conducted to explore how carefully designed surface morphological metrics and the Weber number can affect droplet splashing behavior, based on which the deposition state diagrams were constructed. Critical droplet velocities for different sized droplets impacting on surfaces featuring different roughness that can prevent splashing, have also been determined to guarantee the protection and aesthetics of the coating surface.

2. Modeling and simulation methods

As previously stated, despite the popularity of research on impacting droplets, few focused on droplet splashing on randomly rough surfaces, and almost none used non-Newtonian droplets. In real-life, however, majority surfaces are randomly rough, and common fluids used in industrial processes are non-Newtonian. Thus, identification of the breakup threshold of a non-Newtonian droplet on randomly rough surfaces would be of great significance to many manufacturing steps. This work contains comprehensive simulations of non-Newtonian droplets on randomly rough surfaces, which are used to determine the effects of surface roughness on the behavior of the droplet upon impact, more specifically, fingering or receding breakup of the droplet.

2.1. Governing equations

For incompressible fluids, conservation equations of mass and momentum govern the fluid flow:

$$\nabla \cdot \boldsymbol{u} = 0 \tag{5}$$

$$\rho \frac{\partial \boldsymbol{u}}{\partial \boldsymbol{t}} + \rho(\boldsymbol{u} \cdot \nabla)\boldsymbol{u} = \nabla \cdot [-p\boldsymbol{I} + \mu(\nabla \boldsymbol{u} + \nabla \boldsymbol{u}^T)] + \boldsymbol{F} \tag{6}$$

where, $\boldsymbol{u}$ represents the velocity, $m \cdot s^{-1}$; p is the pressure, Pa; and $\boldsymbol{F}$ is the external volume force that acts on the fluid, $N \cdot m^{-3}$.

A phase field method is adopted to track droplet surface during the impacting process. The liquid–gas interface is tracked by the Cahn-Hilliard equation (Cahn and Hilliard, 1958; Liu et al., 2013; Xiao and Chaudhuri, 2012):

$$\frac{\partial \phi}{\partial t} + \boldsymbol{u} \cdot \nabla \phi = \nabla \cdot (M \nabla G) \tag{7}$$

where ϕ is the dimensionless phase field variable, M is the mobility, $m^3 \cdot s \cdot kg^{-1}$, and G is the chemical potential, Pa. Detailed equations for the phase field method can be found in Xiao et al. (2018).

2.2. Initial and boundary conditions

To better track the gas–liquid and liquid–solid interfaces during the process of droplet impact on the randomly rough surface, the mesh of the domain contains very fine grids on and adjacent to the rough surface for capturing droplet impact dynamics (see Fig. 1).

In this study, the size of the simulation domain is 180 μm × 60 μm. The surface has a non-uniform morphology, so for each specific case, a total of five simulations were conducted with five different droplet impact locations: i.e., 3 μm and 6 μm to the left side, central position and, 3 μm and 6 μm to the right side (Fig. 1(b)).

The initial air–liquid interface (i.e., the boundary between air and liquid) is plotted as the dashed line in Fig. 1(b). This boundary changes as the liquid moves. Air inlets were applied to the left boundary, and air outlets were applied to the right and top boundaries. The air inlet velocity is set as 0. The wettability of the bottom rough surface is determined by setting the intrinsic contact angle and the physical morphology of the surface. The intrinsic contact angle is θ_b, and the physical topography of the surface is directly plotted in the geometry of the simulation system (Fig. 1).

The initial velocity of the droplet is 0. To obtain a specific velocity at which the droplets impact the surface, a temporary volume force is applied to the liquid droplet before impacting the wall, expressed as:

$$F = \rho_2 \cdot \left(\frac{\frac{1}{2} \cdot u_0^2}{h} - g \right) \tag{8}$$

where ρ_2 is the density of the droplet, $kg \cdot m^{-3}$; u_0 is the velocity of the droplet when it first touches the surface, $m \cdot s^{-1}$; h is the distance travelled by the droplet upon impact, m (set at 25 μm); and g is the gravitational acceleration of the droplet, $m \cdot s^{-2}$. It should be pointed

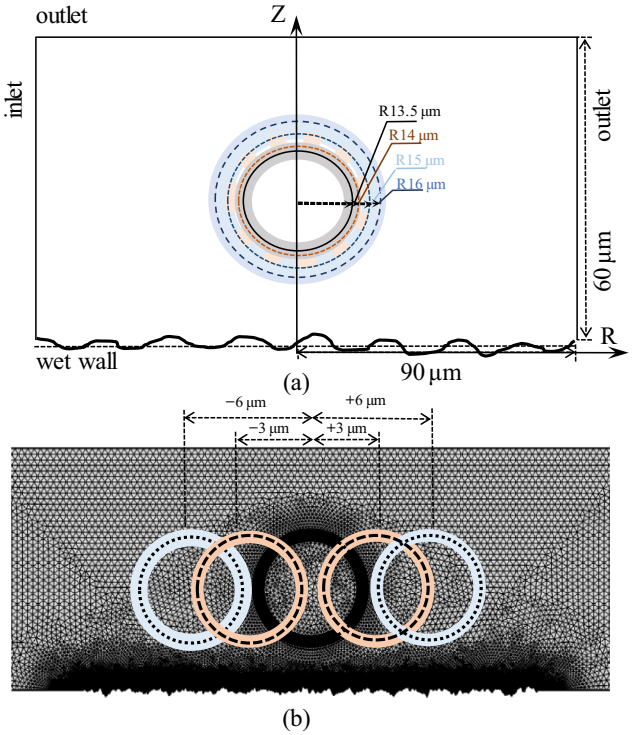

Fig. 1. The simulation system: (a) computation domain with boundary conditions, and (b) the mesh grid together with five different droplet initial locations.

out that the volume force is removed once the droplet impacts the surface.

2.3. The properties of the droplet

In this work, paint droplets were used as the tested non-Newtonian liquid in the simulation. It is a metallic automotive waterborne basecoat, i.e., a real paint whose rheological properties are thoroughly reported by Xu and Koelling (2005). Table 1 lists the specific parameter values of the droplet and surface properties used in this paper. The initial droplet diameter (D_0) ranges from 27 μm to 32 μm, and it is positioned 25 μm above the rough surface (see Fig. 1(a)). The density and surface tension are, respectively, 1080 kg·m^{-3} and 0.02 N·m^{-1}. The intrinsic contact angle of the surface θ_b is 80°. An additional volume force F (N·m^{-3}) was exerted on the droplet to achieve the impact velocity of 7 ~ 16 m·s^{-1}.

According to Eq. (1), droplet diameter and its impact velocity can be designed to offer desirable Weber numbers. Fig. 2 shows all settings of the diameter and the corresponding impact velocity adopted in this work. Each symbol in the figure corresponds to the settings in one in silico experiment.

It should be noted that, in addition to the shear-thinning behavior, a paint material may demonstrate thixotropy and viscoelasticity. For the particular paint under an operational temperature of 20 °C investigated in this work, however, the thixotropy and viscoelasticity can be neglected. The shear viscosity in relation to the shear rate is described by the power-law equation (Xu and Koelling, 2005):

$$\mu = m\left(\frac{\partial u}{\partial y}\right)^{n-1} \tag{13}$$

where m is the consistency coefficient (Pa·s^n) and n is the shear-thinning behavior index. The droplet viscosity decreases as shear-rate increases for the entire range. Fig. 3 shows the viscosity of the shear-thinning droplet.

2.4. Characterization of the randomly rough surface

The aim of this work is to investigate how the topography of randomly rough surfaces can affect droplet breakup behavior. Weierstrass-Mandelbrot (W-M) fractal function was used to create the randomly rough surfaces in this work (Fu et al., 2017). This function allows us to construct surfaces with two types of well-defined roughness.

Root-mean-square roughness in μm, Rr, is defined as,

$$Rr = \sqrt{\frac{\sum_{i=1}^{n}(h_i - \bar{h})^2}{n}} \tag{14}$$

where $\bar{h}$ is the mean height of all n sampling points on the surface.

Wenzel roughness, Wr, is the ratio of liquid–solid contact area to its projected area,

$$Wr = \frac{S}{S_0} \tag{15}$$

Wenzel roughness (Wr) and root-mean-square roughness (Rr), as quantitative metrics of specific surface topography, are the two most widely used methods to characterize rough surfaces. Our work makes it possible to independently study the effects of Wr and Rr on droplet breakup, which is one of the major contributions of this work. The surfaces under investigation are plotted in Fig. 4 with Wr and Rr clearly indicated.

Table 1
Properties of the droplet and the surface.

Properties	Values
Temperature/℃	20
Diameter/μm	27 ~ 32
Density/kg·m^{-3}	1080
Impact velocity/m·s^{-1}	7 ~ 16
Surface tension/N·m^{-1}	0.02
Intrinsic contact angle/°	80
Non-Newtonian viscosity/Pa·s	m:0.3485 n:0.648

2.5. Design of in silico experiments and data analysis method

Both the Weber number and the surface roughness play a major role in influencing droplet breakup. As can be seen from Eq. (1), there are multiple ways of changing We. One of the methods is to change only the impact velocity, and the other method is to change the impact velocity along with the droplet diameter to get the same We as in the former method. In this work, to demonstrate the generality of the findings, the two methods were both adopted to change the Weber number. The combinations of impact velocity and droplet diameters deigned in this work are given in Fig. 2. According to the W-M function, nine rough surfaces were constructed (see Fig. 4). The five surfaces on the left side have the same Wr but different Rr. The right side five have the same Rr but different Wr. Due to the irregular surface structure, five initial droplet locations were simulated for each set of simulation on a surface. In order to identify critical We (i.e., breakup threshold) for a surface, 13–15 groups of simulations with different We values were designed. In total, 1350 in silico experiments were performed, i.e., 130 to 150 simulations for each surface.

Deposition state diagram. When a droplet splits during the spreading process to form secondary droplets, a fingering splash occurs. When a droplet is broken up during the receding phase, a receding breakup occurs. The computation can be terminated after the detection of a breakup. Otherwise, the droplet is non-splashing. These three types of deposition state of the droplet can be plotted in a Weber number vs. surface roughness figure, which is the deposition state diagram. Note that for a specific Weber number and a specific roughness, there are 10 in silico experiments. Five of them correspond to five impact locations with a Weber number designed by varying the impact velocity only and the other five correspond to a Weber number designed by varying both impact velocity and droplet diameter. It should be emphasized that the corresponding We for a specific deposition state can be determined only when all 10 experiments result in the same droplet deposition state.

Critical impact velocity. Based on the deposition state diagram, the critical We, below which a non-splashing state can be ensured, as a function of surface roughness can be identified. In many applications, droplet breakup needs to be avoided. It is useful to offer critical impact velocity for certain-sized droplet on surfaces with certain roughness.

$$u_{0,c} = \left(\frac{\sigma \cdot We_c^{max}}{\rho \cdot D_0}\right)^{1/2} \tag{16}$$

where We_c^{max} is the critical Weber number identified from the deposition state diagram.

2.6. Simulation and analysis procedure

To quantitatively explore breakup behavior of a non-Newtonian droplet on randomly rough surfaces, a general procedure is listed below.

Step 1: Design of in silico experiments. Based on the size of droplets under investigation, determine the size of the simulation

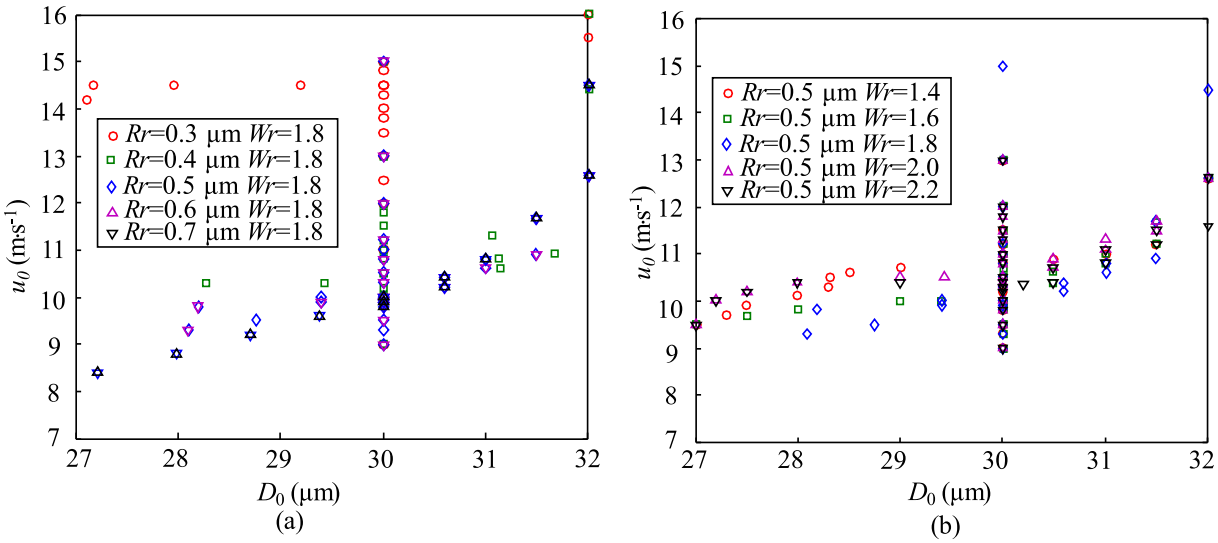

Fig. 2. Settings of the droplet diameter and the impact velocity adopted in this work: (a) for cases with different R_r, and (b) for cases with different W_r.

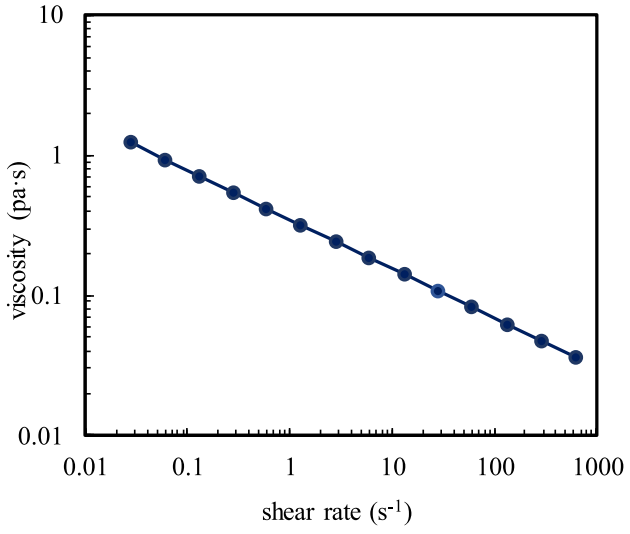

Fig. 3. Shear thinning behavior of the paint droplet.

domain that can accommodate the deformed droplet impacted on the surface. The randomly rough surfaces can be constructed according to the W-M fractal function (see Fig. 4). Droplets' diameter and impact velocity are systematically designed in order to explore a desirable range of Weber numbers (see Fig. 2). At the same time, for the shear-thinning fluid, obtain values of the consistency coefficient and power law index in the viscosity model (i.e., Eq. (13)).

Step 2: Simulation of droplet impact process. The dynamic splashing process of shear-thinning droplets on randomly rough surfaces can be modeled using the phase field method (Eq's. (5)–(7)). Simulations were carried out using COMSOL Multiphysics software (COMSOL, 2018). Multiple initial locations of the droplet are adopted for a case with a specific combination of droplet size and impact velocity so that all geometric features of an irregular surface can be sampled (see Fig. 1(b)). Desirable impact velocities can be achieved by implementing a temporary body force calculated by Eq. (8).

Step 3: Generation of the deposition state diagram. The output from each in silico experiment is the fate (i.e., the deposition state) of the droplet after the impact. As mentioned earlier, one of the three states, i.e., fingering splash, receding breakup and non-splashing, identified from the simulation is recorded as the output. Carrying out all in silico experiments offer a series of state data. A deposition state diagram is generated by plotting these states using specific symbols in a Weber number vs. roughness figure.

Step 4: Identification of the critical Weber number. Based on the deposition diagram constructed in Step 3, for each surface roughness (either *Rr* or *Wr*), identify the maximum *We* that can offer non-splashing states for all in silico experiments designed for that specific *We*. It is a critical Weber number, We_c^{max}, below which a non-splashing state can be ensured. Similarly, identify the minimum *We* that can offer all fingering splash states. This is the other critical Weber number, We_c^{min}, above which a fingering splash can be ensured. After connecting all critical Weber numbers by lines, the deposition state diagram is divided into three zones. The zone below We_c^{max} corresponds to a non-splashing state and the zone above We_c^{min} corresponds to a fingering splash state, while the middle zone is a transition zone within which three states coexist.

Step 5: Identification of the critical impact velocity. Given the surface roughness and the size of the impacting droplet, a critical impact velocity can be calculated by Eq. (16). Droplet impact velocity needs to be controlled below the critical velocity in order to ensure a non-splashing state.

3. Results and discussion

The simulation and analysis method introduced in the previous section is general and can be applied to a variety of processes involving droplet deposition. The phase field model was validated by experimental results reported in German and Bertola, 2009. Detailed validation results as well as parameter settings are presented in the Appendix. Paint droplet deposition for coating formation is selected in this work to demonstrate the capability of the developed approach. Splashing of droplets should be avoided for achieving decent coating quality (Li et al., 2007). The properties of paint droplets are given in Table 1. The geometry of the simulation system is displayed in Fig. 1. The 2D simulation box has a length of 180 μm and a height of 60 μm. The bottom rough surface is one of the Self-affine fractal surfaces in Fig. 4. In this section, the effects of the two types of surface roughness on the droplet splashing behavior are discussed and summarized. Moreover, we will

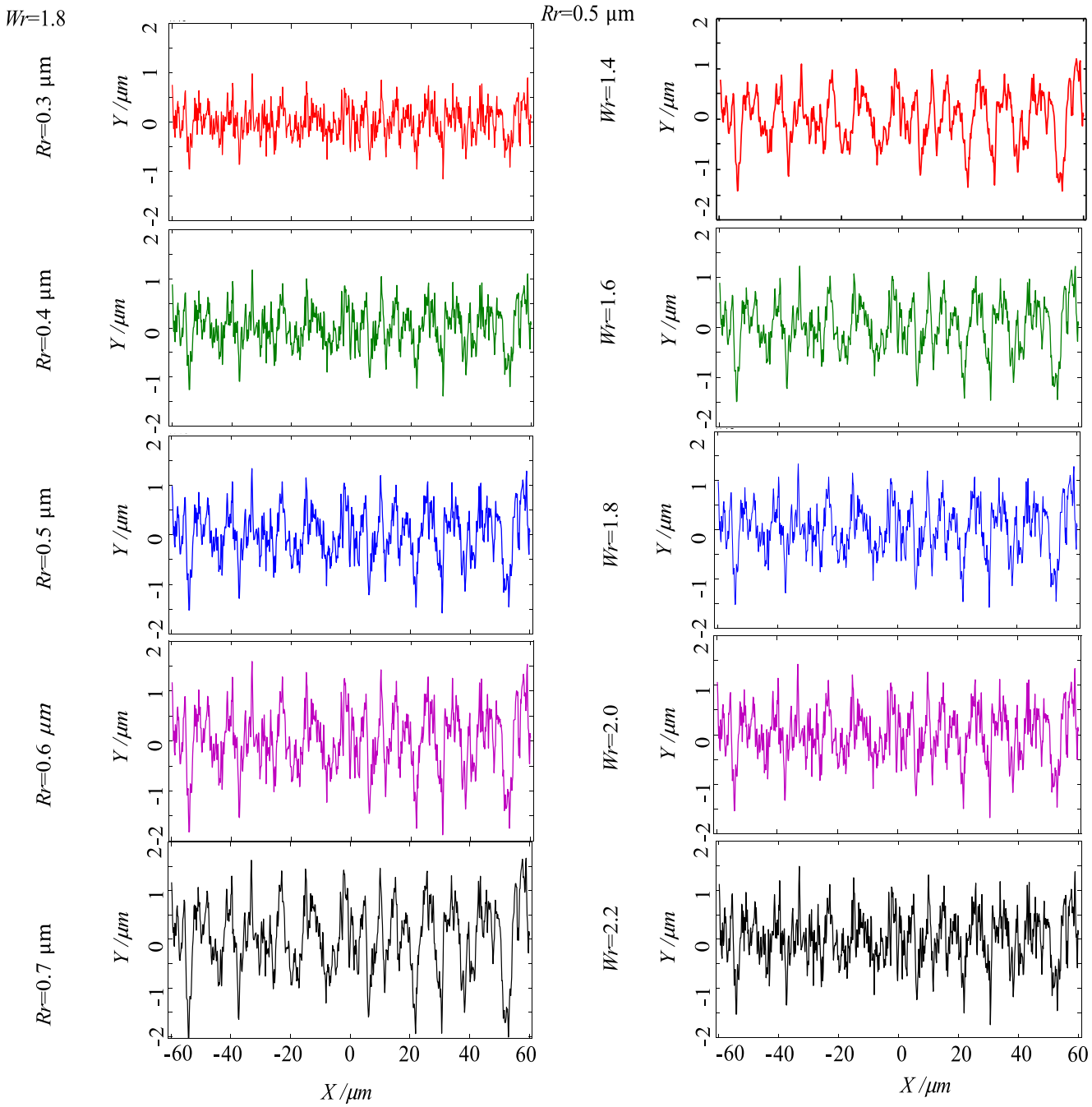

Fig. 4. Self-affine fractal surfaces (left column: surfaces with different *Rr* but the same *Wr*, right column: surfaces with different *Wr* but the same *Rr*).

show how one can prevent droplet splashing, by controlling the surface roughness, droplet size, together with its impact velocity.

3.1. Effect of Weber number on droplet breakup

In this work, a surface with *Rr* = 0.5 μm and *Wr* = 1.8 is selected as a base case surface. In silico experiments were carried out. Representative deposition dynamics are given in Fig. 5.

As can be seen in Fig. 5, a droplet of 30 μm deforms once it impacts on the rough surface. Due to the shear thinning property of the fluid, the large shear stress during the spreading process deforms the droplet to almost a flat plate with two rims. After reaching the maximum spreading, the droplet begins to recede back. When the impact velocity is 9.3 m/s, no breakup can be observed. Increasing the velocity to 10 m/s, two tiny secondary droplets can be identified adjacent to the bulk droplet during the receding stage, indicating receding breakup. Further increase of velocity to 11.2 m/s leads to the separation of two rims (or fingers) from the bulk droplet during the spreading stage. These results show that increasing Weber number can lead to the deposition state transition from non-splashing to receding breakup and further to fingering splash.

To quantitatively evaluate the effect of Weber number on deposition state, a series of in silico experiments were conducted whose results are given in Fig. 6. The following discussions are based on the results for the base case surface with *Rr* = 0.5 μm and *Wr* = 1.8 (see the symbols in the middle column of Fig. 6). For each specific Weber number, 10 symbols can be identified as results

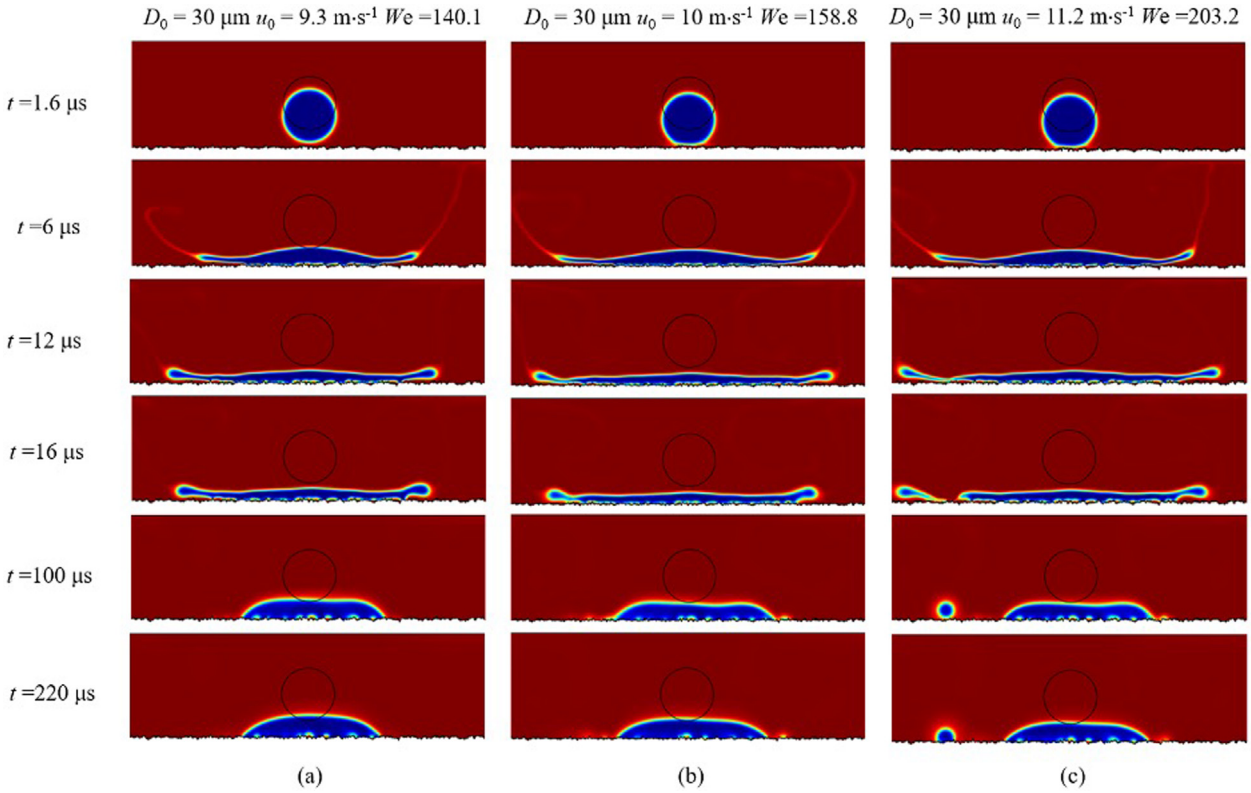

Fig. 5. Deposition dynamics of shear-thinning droplets on a random rough surface (*Rr* = 0.5 μm and *Wr* = 1.8) under different Weber numbers: (a) non-splashing, (b) receding breakup during the receding phase, and (c) fingering splash during the spreading phase.

from 10 in silico experiments. These 10 simulations can be divided into two groups, i.e., five simulations in each group corresponding to five different droplet impact locations on the same surface (see Fig. 1(b)). The series of left 5 symbols corresponds to the change of the initial impact velocity as a means to alter the Weber number, with the droplet diameter held constant at 30 μm, and the droplet impact velocity ranging from 7 m·s^{-1} to 16 m·s^{-1}. The series of the right 5 symbols corresponds to the cases by changing both the initial impact velocity and the droplet diameter to get the same *We* as the left 5 symbols. When *We* is sufficiently high, as shown in Fig. 5 (c), the fingers will form at the periphery of an expanding lamella after the droplet impacts the surface at *t* = 12 μs. Due to the high outward momentum of the fingers, they then break, resulting in secondary droplets which shed out from the rim (see Fig. 5(c)). The critical *We*, We_c^{min}, can be identified as 203.2; for the corresponding left 5 star symbols (Fig. 6), the droplet diameter is

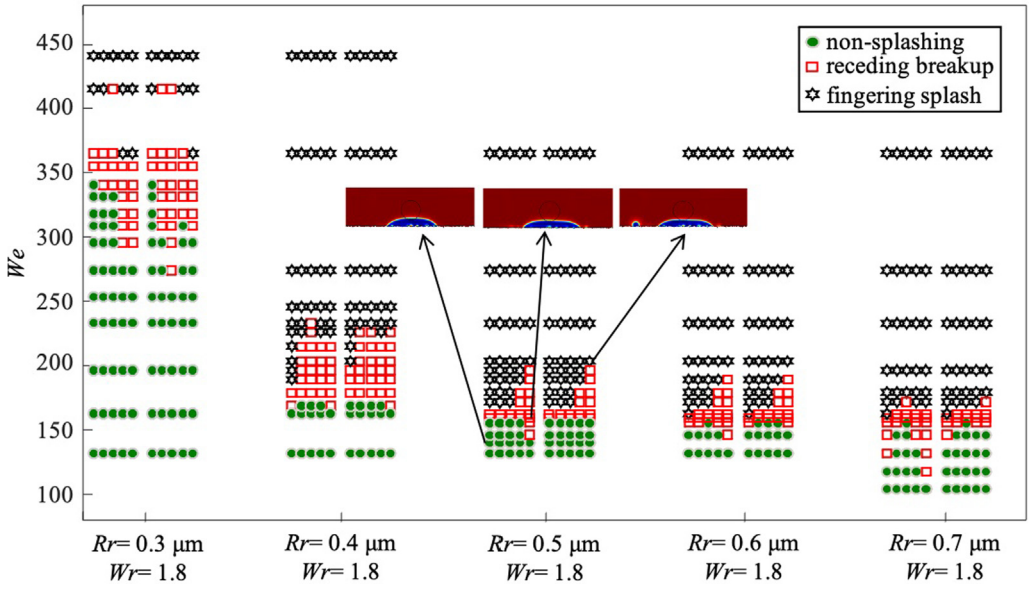

Fig. 6. Deposition state diagram for shear-thinning droplets impacting on surfaces with different *Rr* but the same *Wr*. The insets show the final droplet shape after the impact for three representative in silico experiments.

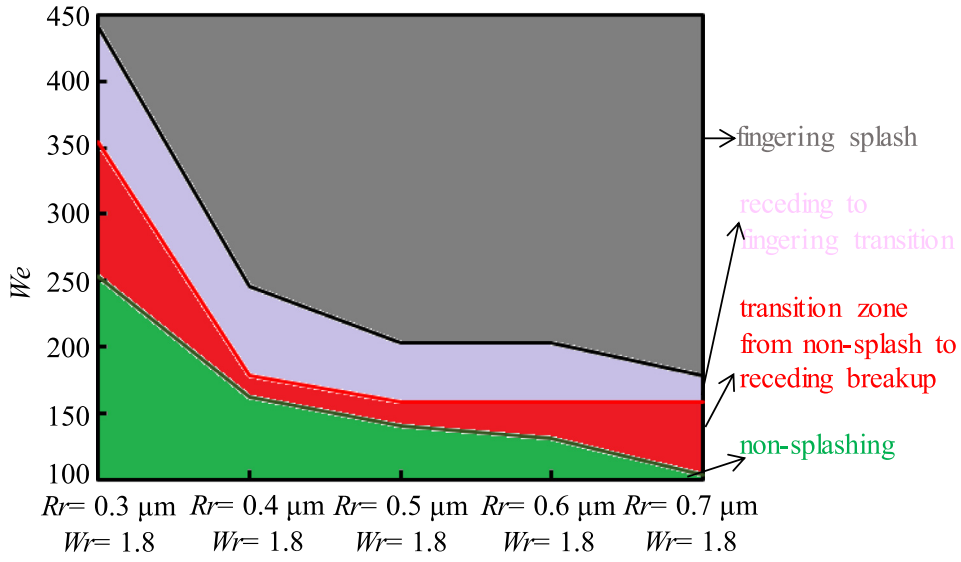

Fig. 7. Critical Weber numbers as a function of *Rr* for shear-thinning droplets impacting on randomly rough surfaces. The green, red, violet and gray zones correspond respectively to non-splashing, transition I (non-splashing to receding breakup), transition II (receding breakup to fingering splash), and fingering splash states. (For interpretation of the references to colour in this figure legend, the reader is referred to the web version of this article.)

30 μm and the impact velocity is 11.2 $m{\cdot}s^{-1}$, and for the right 5 stars, the diameter is 31.5 μm and the impact velocity is 10.9 $m{\cdot}s^{-1}$. When *We* is lower than the critical value, We_c^{max}, 140.1, only non-splashing state can be identified (see Fig. 6). Droplets experience two phases, the spreading phase, and the receding phase to reach an equilibrium state (see Fig. 5(a) for the corresponding morphological evolution of the impacting droplets). Corresponding parameters of droplets for 10 green dot symbols at *We* = 140.1 (see Fig. 6), are respectively 30 μm, 9.3 $m{\cdot}s^{-1}$ and 28.75 μm, 9.5 $m{\cdot}s^{-1}$. In between $We_c^{min} = 203.2$ and $We_c^{max} = 140.1$, three states are all possible. At *We* = 158.8, ten in silico experiments offer the same output, which is the receding breakup state (see Fig. 6). The left five square symbols have the parameters of 30 μm and 9.9 $m{\cdot}s^{-1}$, and the parameters of the five symbols on the right are 29 μm and 10 $m{\cdot}s^{-1}$. Droplets will breakup during the receding phase. The outer rim of the droplet cannot follow with the center of the droplet to retract to an equilibrium state, resulting in a receding breakup. In this special region from $We_c^{max} = 140.1$ to $We_c^{min} = 203.2$, droplet deposition state transits from non-splashing to receding breakup and further to fingering splash.

3.2. Effect of root-mean-square roughness on droplet breakup

Surface structure is another important factor affecting droplet breakup. In this work, in addition to the base case surface, eight additional randomly rough surfaces (see Fig. 4) were investigated

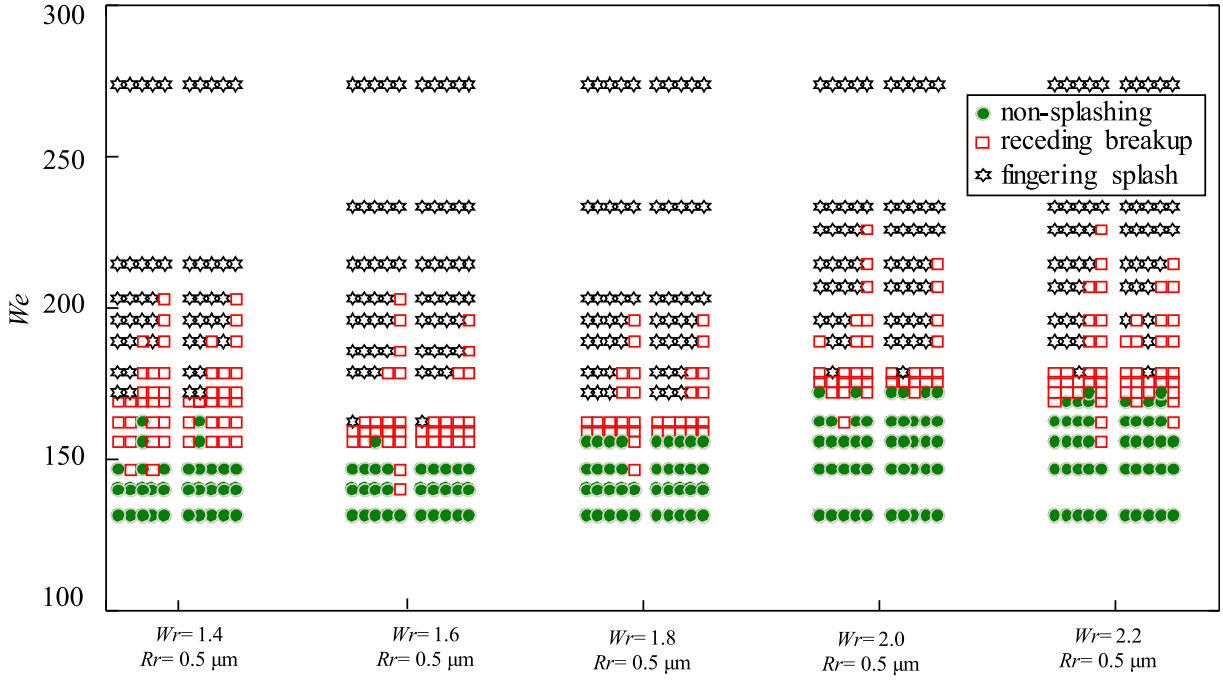

Fig. 8. Deposition state diagram for shear-thinning droplets impacting on surfaces with different *Wr* but the same *Rr*.

to explore the effects of surface roughness on droplet deposition dynamics. In this section, the five surfaces to be compared have the same *Wr* but different *Rr* (the left set of surfaces in Fig. 4).

After running all in silico experiments, the deposition state diagram can be generated (see Fig. 6). The influence of Weber number on droplet breakup does not change with the roughness. For all surfaces, increasing *We* leads to transition of deposition state from non-splashing to receding breakup and further to fingering splash. However, change of the root-mean-square roughness *Rr* has significant impact on critical Weber numbers. A larger surface roughness results in lower critical Weber numbers, i.e., a more effortless breakup. The *Rr* roughness promotes droplet breakup. As shown in Fig. 4, an increase of the root-mean-square roughness enlarges the size of the gaps between peaks, which increases the volume of air trapped under a droplet during impact, thus increasing the likelihood of breakup.

Linking critical Weber numbers by lines as described in *Step 4* (see Section 2.6) yields Fig. 7. In addition to We_c^{max} and We_c^{min}, the Weber number offering ten receding breakup outputs are also connected. In this way, two transition zones can be identified. As shown in Fig. 7, the red zone indicates a transition (i.e., transition I) from non-splashing to receding breakup and the violet zone corresponds to a transition (i.e., transition II) from receding breakup to fingering splash. Deposition in the gray and green zone result in respectively fingering splash and non-splashing state. By resorting to this diagram, the fate of shear-thinning droplets impacting on randomly rough surfaces can be quantitatively identified. Fig. 7 also shows that both We_c^{max} and We_c^{min} decreases drastically with the increase of *Rr*, implying that droplet breakup favors surfaces with high root-mean-square roughness.

3.3. Effect of Wenzel roughness on droplet breakup

In order to investigate the effects of Wenzel roughness, *Wr*, on droplet deposition dynamics, the root-mean-square roughness *Rr* was kept constant while various cases of *Wr* were considered. Five surfaces are shown in Fig. 4 (the right column). Deposition state diagram for changing *Wr* from 1.4 to 2.2 with *Rr* fixed at 0.5 μm is shown in Fig. 8. It can be observed in Fig. 8 that, an increase in *We* will cause the droplet to more easily breakup on each surface.

It is interesting to note that, different from *Rr*, change of Wenzel roughness *Wr* has far less influence on critical Weber numbers (see comparison between Fig. 7 and Fig. 9). Despite both types of roughness have been conventionally adopted for rough surface characterization, they demonstrate distinct influences on droplet breakup. Our findings indicate the necessity to differentiate these two characterizations of surface structure in the study of droplet impact process.

3.4. Critical impact velocity for ensuring a non-splashing state on randomly rough surfaces

Although Fig's. 7 and 9 offer comprehensive deposition state data, Weber number is not a straightforward variable that can be manipulated by engineers overseeing the process in a real production. According to Step 5 (see Section 2.6), one can obtain the maximum velocity at which droplets can impact the surface without breakup.

Plotting the critical impact velocity as a function of root-mean-square roughness and the droplet diameter yields a 3D surface plot as shown in Fig. 10(a). Similarly, the other 3D plot can be generated when the substrate surface varies in Wenzel roughness (Fig. 11(a)). Corresponding 2D plots are Fig. 10(b) and Fig. 11(b), which show how can surface roughness influence critical impact velocity for different sized droplets. It can be concluded that for any specific rough surface under investigation in this work, larger droplets tend to break up more easily as compared with smaller droplets, hence larger droplets demonstrate lower critical impact velocities (Fig. 10 and Fig. 11). Moreover, the critical impact velocity is far more sensitive to the root-mean-square roughness than to the Wenzel roughness regardless of the size of the droplet (see comparison between Fig. 10 and Fig. 11). A surface with higher root-mean-square roughness has a lower critical impact velocity, implying easier droplet breakup (see Fig. 10). By resorting to these plots, engineers, once know the surface roughness and the droplet diameter, can easily prevent breakup of droplets upon impact by maintaining their impact velocity lower than the corresponding critical values. This quantitative information is of great convenience for engineers to control processes involving droplet impact on rough surfaces.

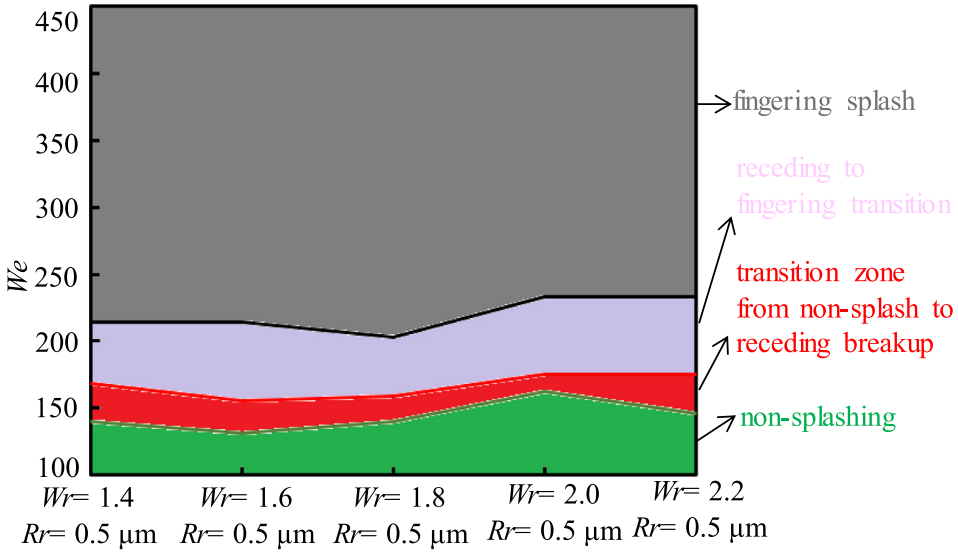

Fig. 9. Critical Weber numbers as a function of *Wr* for shear-thinning droplets impacting on randomly rough surfaces. The green, red, violet and gray zones correspond respectively to non-splashing, transition I (non-splashing to receding breakup), transition II (receding breakup to fingering splash), and fingering splash states. (For interpretation of the references to colour in this figure legend, the reader is referred to the web version of this article.)

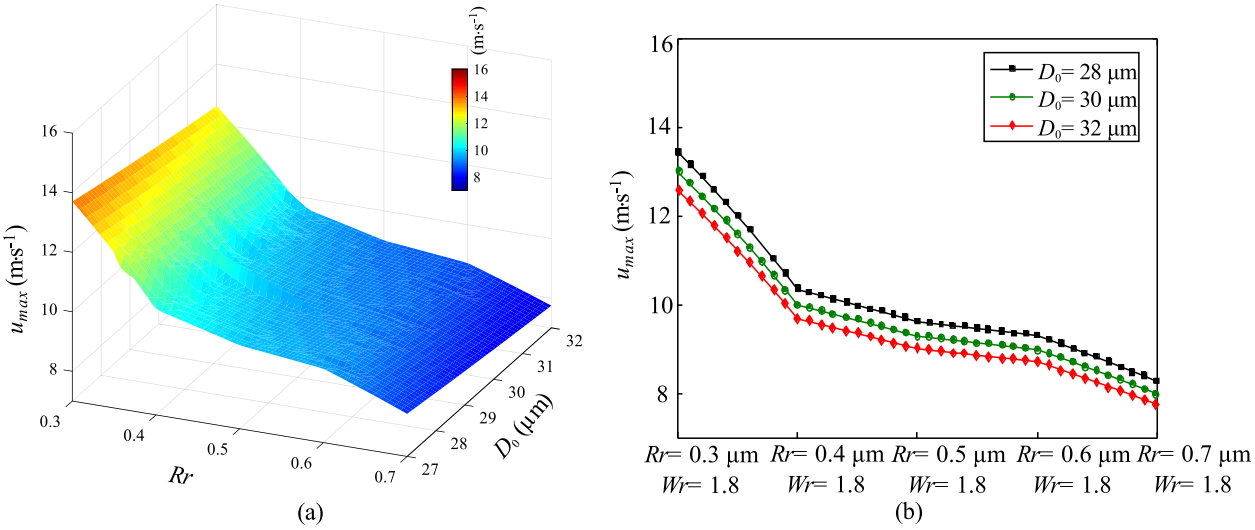

Fig. 10. Critical impact velocity of droplets impacting on a randomly rough surface as a function of root-mean-square roughness and the droplet diameter: (a) a 3D plot and (b) a 2D plot.

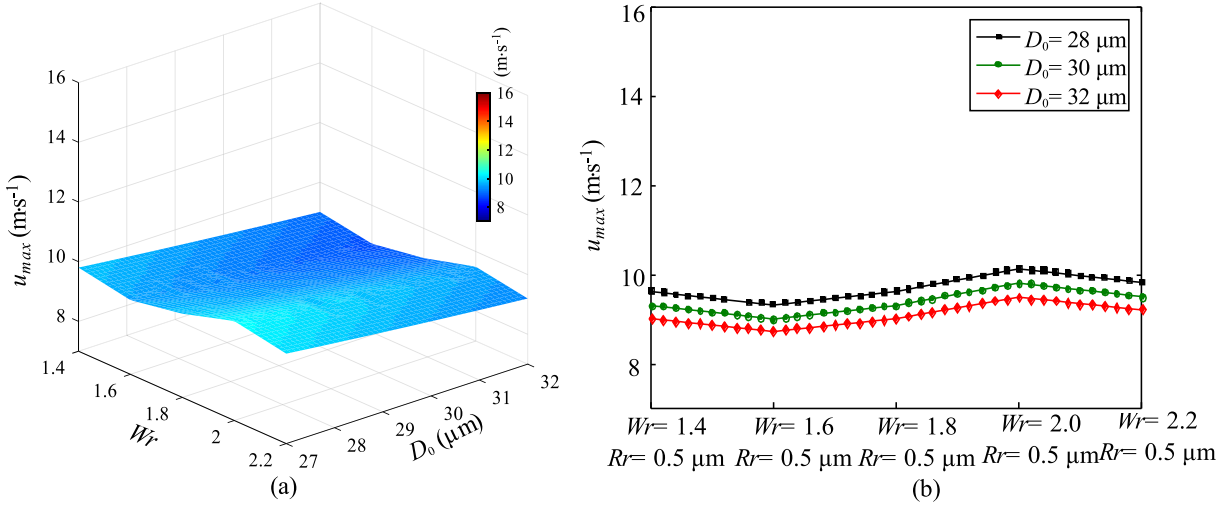

Fig. 11. Critical impact velocity of droplets impacting on a randomly rough surface as a function of Wenzel roughness and the droplet diameter: (a) a 3D plot and (b) a 2D plot.

4. Conclusion

In this work, the breakup threshold of droplets impacting on rough surfaces has been quantitatively investigated by resorting to multiphase flow CFD simulations. Unique contributions of this effort are summarized below: (1) The system explored is shear thinning droplets impacting on randomly rough surfaces, which is a representative system in nature and many industrial applications, but lacks even preliminary study. (2) Specially designed randomly rough surfaces allowed us to differentiate the effects of the root-mean-square roughness (*Rr*) and the Wenzel roughness (*Wr*) on droplet breakup upon impact. (3) A depositions state diagram was constructed based on a large number of systematically designed in silico experiments. (4) Critical Weber number and critical impact velocities have been identified for surfaces with different morphologies, which can greatly facilitate the control of droplet deposition state.

Simulation results show that the Weber number and surface morphology both influence the droplet deposition process. For any specific surface, increasing Weber number leads to the transition of deposition state from non-splashing to receding breakup, and further to fingering splash. Larger droplets break up more readily as compared with smaller droplets, which is evidenced by the lower critical impact velocities demonstrated by larger droplets. Interestingly, both critical Weber number and critical impact velocity are far more sensitive to *Rr* than to *Wr* regardless of the size of the droplet. Thus, it is *Rr* rather than *Wr* that can effectively manipulate droplet deposition state. Increasing *Rr* promotes splashing.

In the future, the model can be extended to the study of droplet impact on 3D randomly rough surfaces. It will be worthwhile to explore droplets with different material properties, e.g., different flow consistency index and flow behavior index, and even different thixotropic and viscoelastic behaviors. Furthermore, challenging

task of establishing empirical equations of critical Weber number and critical impact velocities as a function of droplet size, property and surface roughness will be pursued.

Author contributions

Prof. Jie Xiao conceptualized the project, designed the simulation cases, developed analysis methods, analyzed the data and revised the manuscript. Ms. Hongtao Xia carried out simulations, analyzed the data and drafted the manuscript. Ms. Xiaofang Zhang carried out simulations and analyzed the data.

Declaration of Competing Interest

The authors declare that they have no known competing financial interests or personal relationships that could have appeared to influence the work reported in this paper.

Acknowledgements

We are grateful for the financial support from the National Natural Science Foundation of China (21978184), the "Jiangsu Innovation and Entrepreneurship (Shuang Chuang) Program", the "Jiangsu Specially-Appointed Professors Program", and the "Priority Academic Program Development (PAPD) of Jiangsu Higher Education Institutions". We appreciate Mr. Chen Liang, an undergraduate student from University of Waterloo, for polishing the language of the manuscript draft.

Appendix. Model validation

To validate the phase field model in this work, numerical simulation of the impact dynamics of a non-Newtonian droplet on a smooth surface was carried out. The experimental data are from German and Bertola (2009). The fluid is the xanthan gum solution with a solute mass fraction of 0.5 wt%. The density of this fluid is 1000 kg/m^3 and the surface tension is 0.07 N/m. It's shear-thinning behavior can be described by the power law model (i.e., Eq. (13)) with a consistency coefficient of 2.846 Pa·s$^{0.129}$ and a power law index of 0.129. A 3.42 mm droplet impacts on a parafilm surface, whose roughness is only about 42–51 nm and the equilibrium contact angle is 95°. The impact velocity is 0.92 m/s, which corresponds to a Weber number of 41. The same trend of the spreading ratio evolution between the model prediction and experimental data can be observed in Fig. A1. The model performs especially well in predicting the maximum and the final equilibrium spreading ratios.

In the Cahn-Hilliard equation (i.e., Eq. (7)), the mobility governs the diffusion-related time scale for the interface, whose value should be appropriately determined. The mobility can be correlated with the interface thickness as:

$$M = \chi\varepsilon^2 \tag{A1}$$

where χ is the mobility tuning parameter (m·s/kg) and ε is the interface thickness (m). In this work, ε is set to one half of the maximum mesh element size in the region through which the interface travels. Four different values of χ (i.e., 0.1 m·s/kg, 1 m·s/kg, 10 m·s/kg and 100 m·s/kg) were tested. Fig. A2 shows comparisons between model predictions and experimental data.

It is shown that increasing mobility leads to the decrease of the equilibrium spreading ratio, i.e., a less spreading state of the final equilibrium droplet on the surface. The value of mobility influences the maximum spreading ratio as well. The best prediction was achieved when the mobility tuning parameter is 1 m·s/kg (see the blue line in Fig. A2), which was selected for all simulations in this work.

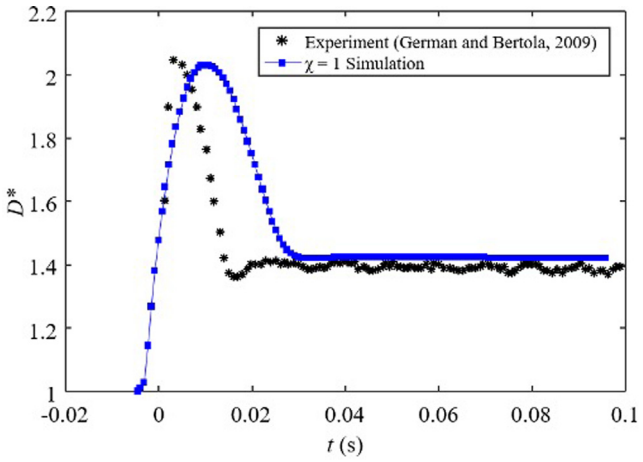

Fig. A1. Evolution of the spreading ratio as a function of time for the 3.42 mm shear-thinning droplet impacting on a parafilm surface with a Weber number of 41. The definition of the spreading ratio can be found in Xiao et al. (2018).

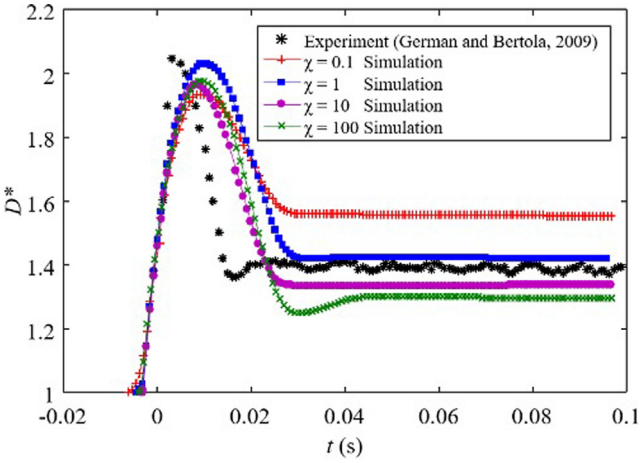

Fig. A2. Evolution of the spreading ratio as a function of time for the 3.42 mm shear-thinning droplet impacting on a parafilm surface with a Weber number of 41: comparison between experimental data and simulation results under different values of mobility tuning parameter.

References

Adam, C.D., 2013. Experimental and theoretical studies of the spreading of bloodstains on painted surfaces. Forensic Sci. Int. 229 (1-3), 66–74.
Allen, R.F., 1975. The role of surface tension in splashing. J. Colloid Interface Sci. 51 (2), 350–351.
Bergeron, V., Bonn, D., Martin, J.Y., Vovelle, L., 2000. Controlling droplet deposition with polymer additives. Nature 405 (6788), 772–775.
Bertola, V., Haw, M.D., 2015. Impact of concentrated colloidal suspension drops on solid surfaces. Powder Technol. 270, 412–417.
Cahn, J.W., Hilliard, J.E., 1958. Free energy of a nonuniform system. I. Interfacial free energy. J. Chem. Phys. 28 (2), 258–267.
Chen, L., Wang, Y., Peng, X., Zhu, Q., Zhang, K., 2018. Impact dynamics of aqueous polymer droplets on superhydrophobic surfaces. Macromolecules 51, 7817–7827.
COMSOL Multiphysics® v. 5.4., 2018. www.comsol.com. COMSOL AB, Stockholm, Sweden..
Cossali, G.E., Coghe, A., Marengo, M., 1997. The impact of a single drop on a wetted solid surface. Exp. Fluids 22, 463–472.

Cossali, G.E., Marengo, M., Santini, M., 2008. Thermally induced secondary drop atomisation by single drop impact onto heated surfaces. Int. J. Heat Fluid Flow 29, 167–177.
Dam, D.B.V., Clerc, C.L., 2004. Experimental study of the impact of an ink-jet printed droplet on a solid substrate. Phys. Fluids 16, 3403–3414.
de Goede, T.C., Laan, N., de Bruin, K.G., Bonn, D., 2018. Effect of wetting on drop splashing of newtonian fluids and blood. Langmuir 34, 5163–5168.
Dong, C., Hao, C., Zhang, X., Cao, C., 2014. Synthesis and characterization of monodisperse copper nanoparticles using gum acacia. Physica E 57, 12–20.
Fu, Y., Zheng, Z., Rui, X., Shi, H., 2017. Comparison of two fractal interpolation methods. Physica A 469, 563–571.
German, G., Bertola, V., 2009. Impact of shear-thinning and yield-stress drops on solid substrates. J. Phys.: Condens. Matter 21, 375111.
Kai, R., Feuillebois, F., 1998. Influence of surface roughness on liquid drop impact. J. Colloid Interface Sci. 203, 16–30.
Latka, A., Strandburg-Peshkin, A., Driscoll, M.M., Stevens, C.S., Nagel, S.R., 2012. Creation of prompt and thin-sheet splashing by varying surface roughness or increasing air pressure. Phys. Rev. Lett. 109, 054501.
Lei, X., Zhang, W.W., Nagel, S.R., 2005. Drop splashing on a dry smooth surface. Phys. Rev. Lett. 94, 184505.
Li, G., Sliefert, N., Michael, J.B., Yarin, A.L., 2021. Blood backspatter interaction with propellant gases. Phys. Fluids 33, 043318.
Li, J., Xiao, J., Huang, Y., Lou, H.H., 2007. Integrated process and product analysis: A multiscale approach to paint spray. AIChE J. 53, 2841–2857.
Li, V.Z., Brunet, P., Eggers, J., Deegan, R.D., 2010. Wavelength selection in the crown splash. Phys. Fluids 22, 24045.
Liu, H., Valocchi, A.J., Zhang, Y., Kang, Q., 2013. Phase-field-based lattice Boltzmann finite-difference model for simulating thermocapillary flows. Phys. Rev. E 87.
Marengo, M., Antonini, C., Roisman, I.V., Tropea, C., 2011. Drop collisions with simple and complex surfaces. Curr. Opin. Colloid Interface Sci. 16, 292–302.
Mehdizadeh, N.Z., Chandra, S., 2004. Formation of fingers around the edges of a drop hitting a metal plate with high velocity. J. Fluid Mech. 510, 353–373.
Moita, A.S., Moreira, A.L.N., 2007. Drop impacts onto cold and heated rigid surfaces: Morphological comparisons, disintegration limits and secondary atomization. Int. J. Heat Fluid Flow 28, 735–752.
Mundo, C., Sommerfeld, M., Tropea, C., 1995. Droplet-wall collisions: Experimental studies of the deformation and breakup process. Int. J. Multiph. Flow 21, 151–173.
Pan, K.L., Tseng, K.C., Wang, C.H., 2010. Breakup of a droplet at high velocity impacting a solid surface. Exp. Fluids 48, 143–156.
Riboux, G., Gordillo, J.M., 2014. Experiments of drops impacting a smooth solid surface: a model of the critical impact speed for drop splashing. Phys. Rev. Lett. 113, 024507.
Roisman, I.V., Lembach, A., Tropea, C., 2015. Drop splashing induced by target roughness and porosity: The size plays no role. Adv. Colloid Interface Sci. 222, 615–621.
Roisman, I.V., Rioboo, R., Tropea, C., 2002. Normal impact of a liquid drop on a dry surface: model for spreading and receding. Proc. Math. Phys. Eng. Sci. 458, 1411–1430.
Smith, F.R., Buntsma, N.C., Brutin, D., 2018. Roughness influence on human blood drop spreading and splashing. Langmuir 34, 1143–1150.
Stow, C.D., Hadfield, M.G., 1981. An experimental investigation of fluid flow resulting from the impact of a water drop with an unyielding dry surface. Proc. Royal Soc. London 373, 419–441.
Tan, H., 2017. Numerical study on splashing of high-speed microdroplet impact on dry microstructured surfaces. Comput. Fluids 154, 142–166.
Thoroddsen, S.T., Etoh, T.G., Takehara, K., Ootsuka, N., Hatsuki, Y., 2005. The air bubble entrapped under a drop impacting on a solid surface. J. Fluid Mech. 545, 203–212.
Wachters, L.H.J., Westerling, N.A.J., 1966. The heat transfer from a hot wall to impinging water drops in the spheroidal state. Chem. Eng. Sci. 21, 1047–1056.
Wal, R.L.V., Berger, G.M., Mozes, S.D., 2006. The splash/non-splash boundary upon a dry surface and thin fluid film. Exp. Fluids 40, 53–59.
Wang, D.M., Watkins, A.P., 1993. Numerical modeling of diesel spray wall impaction phenomena. Int. J. Heat Fluid Flow 14, 301–312.
Wirth, W., Storp, S., Jacobsen, W., 1991. Mechanisms controlling leaf retention of agricultural spray solutions. Pestic. Sci. 33, 411–420.
Xia, H.T., Zou, S.Y., Xiao, J., 2019. Numerical simulation of shear-thinning droplet impacting on randomly rough surfaces. CIESC J. 70, 634–645.
Xiao, J., Chaudhuri, S., 2012. Design of anti-icing coatings using supercooled droplets as nano-to-microscale probes. Langmuir 28, 4434–4446.
Xiao, J., Li, J., Xu, Q., Huang, Y., Lou, H.H., 2010. ACS–based dynamic optimization for curing of polymeric coating. AIChE J. 52, 1410–1422.
Xiao, J., Pan, F., Xia, H., Zou, S., Zhang, H., George, O.A., Zhou, F., Huang, Y., 2018. Computational study of single droplet deposition on randomly rough surfaces: surface morphological effect on droplet impact dynamics. Ind. Eng. Chem. Res. 57, 7664–7675.
Xu, J., Koelling, K.W., 2005. Temperature dependence of rheological behavior of a metallic automotive waterborne basecoat. Prog. Org. Coat. 53, 169–176.
Zhang, D., Papadikis, K., Gu, S., 2014. Application of a high density ratio lattice-Boltzmann model for the droplet impingement on flat and spherical surfaces. Int. J. Therm. Sci. 84, 75–85.